Received: 11 November 2019 | Accepted: 14 February 2020

DOI: 10.1111/ppa.13173



Plant Pathology An International Journal edited by the British Society for Plant Pathology WILEY

ORIGINAL ARTICLE

# Tracking host infection and reproduction of *Peronospora salviae-officinalis* using an improved method for confocal laser scanning microscopy

Mascha Hoffmeister[1] | Wolfgang Maier[1] | Marco Thines[2,3] | Yvonne Becker[1]

[1]Institute for Epidemiology and Pathogen Diagnostics, Julius Kühn Institut (JKI)—Federal Research Centre for Cultivated Plants, Braunschweig, Germany

[2]Department of Biological Sciences, Institute of Ecology, Evolution and Diversity, Goethe University, Frankfurt am Main, Germany

[3]Senckenberg Gesellschaft für Naturforschung, Senckenberg Biodiversity and Climate Research Centre (BiK-F), Frankfurt am Main, Germany

**Correspondence**
Yvonne Becker, Institute for Epidemiology and Pathogen Diagnostics, Julius Kühn Institut (JKI), Federal Research Centre for Cultivated Plants, Messeweg 11/12, 38104 Braunschweig, Germany.
Email: yvonne.becker@julius-kuehn.de

**Funding information**
Federal Ministry of Food and Agriculture

## Abstract

*Peronospora salviae-officinalis*, the causal agent of downy mildew on common sage, is an obligate biotrophic pathogen. It grows in the intercellular spaces of the leaf tissue of sage and forms intracellular haustoria to interface with host cells. Although *P. salviae-officinalis* was described as a species of its own 10 years ago, the infection process remains obscure. To address this, a histological study of various infection events, from the adhesion of conidia on the leaf surface to de novo sporulation is presented here. As histological studies of oomycetes are challenging due to the lack of chitin in their cell wall, we also present an improved method for staining downy mildews for confocal laser scanning microscopy as well as evaluating the potential of autofluorescence of fixed nonstained samples. For staining, a 1:1 mixture of aniline blue and trypan blue was found most suitable and was used for staining of oomycete and plant structures, allowing discrimination between them as well as the visualization of plant immune responses. The method was also used to examine samples of *Peronospora lamii* on *Lamium purpureum* and *Peronospora belbahrii* on *Ocimum basilicum*, demonstrating the potential of the presented histological method for studying the infection processes of downy mildews in general.

KEYWORDS

aniline blue, confocal laser scanning microscopy, *Peronospora belbahrii*, *Peronospora lamii*, *Peronospora salviae-officinalis*, trypan blue

## 1 | INTRODUCTION

The downy mildew *Peronospora salviae-officinalis* causes a severe disease on the medicinal plant *Salvia officinalis* (common sage, Lamiaceae). Since its first report as a *Peronospora* sp. on *S. officinalis* in 1993 (McMillan, 1993), the disease has been reported from all over the world (Gamliel and Yarden, 1998; Hill *et al.*, 2004; Belbahri *et al.*, 2005; Liberato *et al.*, 2006; Humphreys-Jones *et al.*, 2008). It is of increasing economical concern and can be regarded as a newly emerging disease. Although *P. salviae-officinalis* was described 10 years ago (Choi *et al.*, 2009) the infection process has never been studied. Knowledge about the epidemiology and biology of this pathogen is, however, crucial for the development of forecast models, and appropriate combat strategies against it in sage production.

Downy mildews of the genus *Peronospora* are obligate biotrophs, which means that they are dependent on living host cells for nutrition (Thines and Choi, 2016). They belong to the Peronosporaceae within the phylum Oomycota of the kingdom Straminipila (Beakes and

Thines, 2017). The cell walls of oomycetes mainly contain β-(1,3)-glucan, β-(1,6)-glucan, and cellulose (Sietsma *et al*., 1969; Blaschek *et al*., 1992). The β-(1,3)-glucan structures of oomycetes are branched to a variable degree (Yamada and Miyazaki, 1976; Fabre *et al*., 1984). Previous studies have shown that the cell walls of Peronosporales contain up to 85% glucans, mainly glucopyranose and 1,4-linked glucosyl residues, derived from cellulose. In contrast to true fungi, chitin derivates are not present in considerable amounts in cell walls of most oomycetes, especially in Peronosporaceae (Bartnicki-Garcia, 1968). Oomycetes also use β-(1,3)-glucan as a storage polysaccharide, in the form of mycolaminarin, but do not use glycogen, which is the storage polysaccharide of fungi and animals (Clavaud *et al*., 2009). The similar cell wall structure of oomycetes and plants renders fluorescence microscopy challenging and the selectivity of fluorescent dyes to bind specific polysaccharides is low. Aniline blue and trypan blue, deployed in several experiments to detect oomycetes in plant tissue (Hood and Shew, 1996; Donofrio and Delaney, 2001; Gindro *et al*., 2003; Huitema *et al*., 2003; Kortekamp, 2005; Diez-Navajas *et al*., 2007) are also used as dyes in plant histology (Smith and McCully, 1978). Aniline blue has been used as a fluorochrome in fluoresence microscopy to detect callose, a linear β-(1,3)-D-glucan, in plant cells (Stone *et al*., 1984; Eschrich and Currier, 2009), but it also binds to other β-(1,3) glucans (Wood and Fulcher, 1984) and cellulose (Mulisch and Welsch, 2015). All glucans are polysaccharides that consist of D-glucose, so the basic structure of the molecule is the same for all of them. Trypan blue is a benzidine-based, anionic azo dye (Combes and Haveland-Smith, 1982) that binds fungal chitin and glucans (Liesche *et al*., 2015), and reduces the intracellular autofluorescence of NADH and riboflavine (Mosiman *et al*., 1997). Moreover, this dye binds to proteins located in the cytoplasm and in the plasma membrane of organisms (Avelar-Freitas *et al*., 2014).

Previous studies have shown that it is possible to recognize intercellular mycelium and haustoria in samples stained with aniline blue or trypan blue (Donofrio and Delaney, 2001; Diez-Navajas *et al*., 2007). A common problem of these methods is the often, low visual contrast and resolution between plant and oomycete structures in thicker tissues, sometimes necessitating sectioning for a clear localization of the haustoria within the plant tissue (Thines *et al*., 2007). In particular, areas of close host–pathogen interaction, for example, penetration hyphae that pierce the plant cell wall, are difficult to visualize. One of the advantages of confocal laser scanning microscopy (CLSM) is the optical sectioning it permits, reducing the need for mechanical sectioning (Czymmek *et al*., 1994). Because optical sectioning is not limited to a single focal plane confocal images can also be collected in the vertical plane by *z* stacks and combination thereafter allows the precise localization of fungal structures within the host tissue.

Here, we aimed to develop a robust method for CLSM by which oomycetous and plant tissue could be clearly differentiated. This was performed using the example of the previously unstudied infection process of *P. salviae-officinalis* in association with its host, *S. officinalis*. As a method published by Becker *et al*. (2018) for visualization of endophytic fungi seemed to be especially promising for the purpose, it was adapted in this study for oomycetes.

## 2 | MATERIALS AND METHODS

### 2.1 | Plant and fungal material

Infection experiments were carried out using plants of *S. officinalis* inoculated with *P. salviae-officinalis*. Sage plants at the 4-leaf-stage were spray-inoculated with a suspension of freshly harvested conidia in deionized water ($10^4$ conidia/ml). Inoculated plants were incubated in a plant growth chamber (Percival Scientific) at 15 °C, 100% relative humidity, and with 12 hr light/12 hr darkness. The downy mildew isolate used for the experiments was obtained from *S. officinalis* in Freital (Saxony, Germany) and has been maintained on *S. officinalis* in our laboratory at the Institute of Epidemiology and Pathogen Diagnostics of the Julius Kühn Institut (Braunschweig, Germany) since 2017. For comparison of the different staining solutions, leaf samples were taken 7 days after inoculation, when dense sporulation on the lower leaf surface was observed. The staining method was also tested for use with *Peronospora belbahrii* on *Ocimum basilicum* and *Peronospora lamii* on *Lamium purpureum* in a similar manner.

To study and document the infection process of *P. salviae-officinalis* on *S. officinalis* from conidial germination until sporulation, sage plants were inoculated and incubated as described above for 14 days. Leaf samples were taken at 1, 4, 7, and 14 days after inoculation (dai). The downy mildew sample on *L. purpureum* was collected in a field (Braunschweig, Germany), whereas *P. belbahrii* was collected from a basil plant bought in a local supermarket (Braunschweig, Germany).

For staining, leaf pieces of 0.5 × 1.5 cm, excluding the middle vein, were sampled for all specimens examined.

### 2.2 | Fixation and staining

To decolourize infected leaf samples, an ethanol series as described by Bougourd *et al*. (2000) for *Arabidopsis* embryos was used: The leaves were successively incubated in 15%, 50%, 70%, 95%, and 99% ethanol, each for 15 min at room temperature (RT), and then in 99% ethanol overnight at 4 °C; afterwards, the samples were incubated successively in 95%, 70%, 50%, and 15% ethanol, and deionized water (twice), each for 15 min at room temperature. After rehydration, samples were incubated in 10% KOH for 3 hr at room temperature, washed three times in phosphate-buffered saline (PBS; 137 mM NaCl, 2.68 mM KCl, 10 mM $Na_2HPO_4$, 1.76 mM $KH_2PO_4$, pH 7.4) and kept at 4 °C. For staining, PBS was removed and samples were covered with the respective staining solution (c. 300 µl/sample) listed in Table 1. A 1% aniline blue stock solution was prepared by dissolving 10 mg aniline blue diammonium salt (Sigma-Aldrich) in 1 ml deionized water. A 1% trypan blue stock solution was prepared by dissolving 10 mg trypan blue powder (Merck) in 1 ml deionized water. Samples were stained by vacuum infiltration five times for 2 min in a glass desiccator (DWK Life Sciences) as described by Becker *et al*. (2018). To evaluate the autofluorescence of plant and downy mildew cells, decolourized samples were not stained, but analysed by CLSM directly. Due to the high contrast offered by CSLM, destaining of stained samples was not necessary.

**TABLE 1** Composition of staining solutions

| Staining solution | Composition of 1 ml staining solution | | | |
|---|---|---|---|---|
| | 1% aniline blue (µl) | 1% trypan blue (µl) | 2% Tween 20 (µl) | PBS (µl) |
| AB 20 | 20 | – | 10 | 970 |
| AB 40 | 40 | – | 10 | 950 |
| TB 20 | – | 20 | 10 | 970 |
| TB 40 | – | 40 | 10 | 950 |
| AB 20/TB 20 | 20 | 20 | 10 | 950 |

Abbreviation: PBS, phosphate-buffered saline.

## 2.3 | CLSM

To determine the fluorescent properties of aniline blue and trypan blue, and to define the autofluorescence of the samples, lambda scans and CLSM imaging of unstained samples and samples stained with AB 40, TB 40, and AB 20/TB 20, respectively, were performed (Table 1). Lambda scans were captured with a photomultiplier tube PMT2. Lambda scan range and properties are shown in Table 2.

Samples for CLSM were transferred from the staining solution to a droplet of 70% glycerol (Carl Roth) on a microscope slide and covered with a cover slip. Fluorescence was recorded with a confocal laser scanning microscope (TCS SP8; Leica). Images were taken using the HC PLAPO CS2 20×/0.75 IMM objective and the Application Suite X (LAS X; Leica) software for Leica microscopes.

Aniline blue- and trypan blue-stained samples, as well as unstained samples, were excited with the 405 nm diode UV laser and the 561 nm diode-pumped solid-state laser (DPSS). The 405 nm laser was employed to visualize callose (β-1,3-glucan) through its UV light-induced fluorescence with the aniline blue fluorochrome, as reported previously (Stone *et al.*, 1984). The intensity of the 405 nm laser was set at 21.1% for lambda scans and dye evaluation. The 561 nm laser was used to visualize aniline blue- and trypan blue-stained glucans of cell walls and cytoplasm, as well as cytosolic proteins. The intensity of the 561 nm laser was set at 24.7%. Laser intensities were adjusted for visualization of the infection process. The intensity of the 405 nm laser ranged between 15% and 39% and the intensity of the 561 nm laser between 8% and 24.7%. Two photomultiplier tubes (PMT2 and PMT4) and one hybrid detector (HyD3) were used to capture the emission fluorescence of the dyes and the autofluorescence of plant and fungal tissue. Pseudocolours were used to represent specific emission fluorescence. Blue pseudocolour (PMT2, 447–495 nm) was used to visualize aniline blue-stained plant callose, UV-induced trypan blue fluorescence and autofluorescence. Green (HyD3, 593–625 nm) and red (PMT4, 673–749 nm) pseudocolours were used to visualize emission fluorescence from aniline blue and trypan blue and to capture plant autofluorescence. Multichannel images were produced by overlay of all three channels, in which overlapping green (HyD3) and red (PMT4) pseudocolours appear orange. Sequential acquisition in three different channels was carried out, to avoid cross-talk. Images were generated by maximum intensity projection of confocal *z* stacks. Thickness of *z* stacks was adjusted to the area of interest. Single images were taken every 1.5 nm. Adobe Photoshop CS2 was used to enhance both brightness and contrast by 33% for the processed confocal *z* stacks.

**TABLE 2** Lambda scan range and properties for UV laser and for diode-pumped solid-state laser (DPSS)

| Property | 405 nm UV laser | 561 nm DPSS laser |
|---|---|---|
| Detection begins (nm) | 420 | 575 |
| Detection ends (nm) | 780 | 780 |
| Total detection range (nm) | 360 | 205 |
| Detection band width (nm) | 30 | 30 |
| No. of detection steps | 67 | 35 |
| λ-detection stepsize (nm) | 5 | 5 |

# 3 | RESULTS

## 3.1 | Development of an aniline blue/trypan blue based staining method for visualization of in planta downy mildew by CLSM

In the lambda scans of the fixed but unstained samples (Table 2) the excitation with the 405 nm laser showed a weak emission signal between 460 and 540 nm, as well as between 620 and 680 nm (Figure S1). Autofluorescence of the samples was strongest when excited with the 561 nm laser, with emission between 575 and 720 nm and a peak at 665 nm (Figure S2). To distinguish plant cells and intercellular hyphae by UV-induced autofluorescence, very high laser intensities (over 50%) had to be applied. High laser intensities lead to photobleaching, and so microscopic analysis of decolourized but unstained samples is not recommended. The 561 nm laser-induced autofluorescence enabled intercellular hyphae and haustoria to be distinguished from plant cells, but the visual contrast and resolution were poor (Figure 1).

The use of staining solutions AB 20 and TB 20 separately showed low sensitivity, weak resolution, and weak visual contrast. However, AB 40 and TB 40 enhanced the sensitivity. Several authors have reported that commercial aniline blue preparations from different companies vary (Smith and McCully, 1978; Bougourd *et al.*, 2000); therefore, lambda scans were conducted. The lambda scan of a

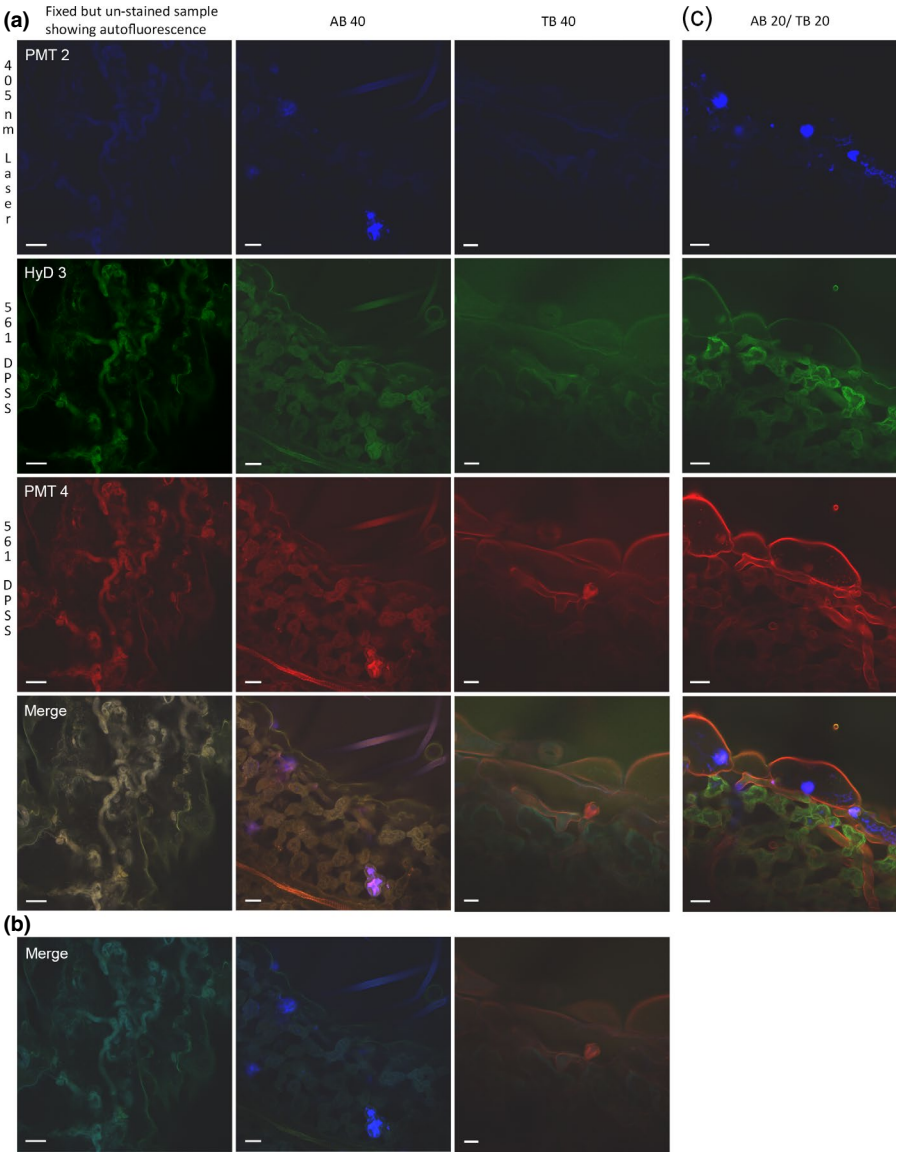


**FIGURE 1** Comparison of different stains for visualization of *Peronospora salviae-officinalis* infections on *Salvia officinalis* and the resulting plant–pathogen interaction 7 days after infection. To compare the sensitivity and performance of the different staining solutions (TB 40, AB 40, AB 20/TB 20) and sample autofluorescence, the confocal laser scanning microscopy (CLSM) acquisition settings used for AB 20/TB 20 were applied. Sequential scans captured with different detectors and merged images of fixed unstained samples, samples stained with aniline blue (AB 40), trypan blue (TB 40), and a 1:1 mixture of aniline blue and trypan blue (AB 20/TB 20) excited with the 405 nm laser and the 561 nm laser are shown. (a) To capture a signal for unstained, AB 40-, and TB 40-stained samples the laser intensity of the 561 nm laser was increased to 35%–42% compared to 24% for the samples stained with the AB 20/TB 20 mixture. (b) Merged images of the sequential scans of unstained, AB 40- and TB 40-stained samples, shown in (a), using the low laser intensity of images shown in (c). (c) Sequential scans and merged image of the sequential scans of samples stained with AB 20/TB 20 mixture. Laser intensity was 21% for the 405 nm laser and 24% for the 561 nm laser. Scale bar represents 20 µm

sample stained with AB 40 showed a strong 405 nm laser-induced signal, with a maximum at 450–480 nm, and a faint signal induced by the 561 nm laser between 640 and 700 nm. The sequential acquisition of each channel revealed that PMT2 (447–495 nm) visualized callose inside the plant tissue and callose accumulations around hyphae and haustoria. Detectors HyD3 (593–625 nm) and PMT4 (673–749 nm) visualized mainly the cytoplasm of plant and oomycete cells, but differentiation between cytoplasm and cell walls was difficult. Visual contrast and resolution provided by AB 40 staining was higher than seen in the unstained samples, but not as high as with TB 40. Staining solution TB 40 showed a faint UV-induced fluorescence in the lambda scan, with a maximum between 640 and 700 nm. The PMT2 captured only background noise in TB 40-stained samples, while the HyD3 captured mainly cytoplasm of plant and oomycete cells and PMT4 visualized mainly cell walls. Using TB 40, intercellular hyphae and haustoria were clearly distinguishable from plant tissue. Visual contrast and resolution provided by TB 40 staining was higher than by AB 40 staining, but callose was not detected.

The lambda scan of the AB 20/TB 20-stained samples using the 405 nm laser showed a first strong emission signal, with a maximum intensity around 460 nm, and a second, fainter, emission signal around 680 nm (Figure S1). Using the 561 nm DPSS laser the detected emission in the lambda scan reached its maximum intensity at 670 nm (Figure S2). The first signal detected with the 405 nm laser was induced by the aniline blue within the staining solution, while the second signal was induced by trypan blue, as lambda scans of AB 40 and TB 40 revealed. Using the 561 nm DPSS laser, the detected emission of AB 20/TB 20 samples reached its maximum at 660 nm. This signal can be attributed to trypan blue. The AB 20/TB 20 treatment showed the highest image resolution. Aniline blue-stained callose deposition and accumulation were visualized in blue pseudocolour (447–495 nm, PMT2); plant and oomycete cytoplasm and plant chloroplasts were visualized in green pseudocolour (593–625 nm, HyD3); and cell walls of host and oomycete were visualized in red pseudocolour (673–749 nm, PMT4). Overall, the background noise of HyD3 and PMT4 was much lower using combined AB 20/

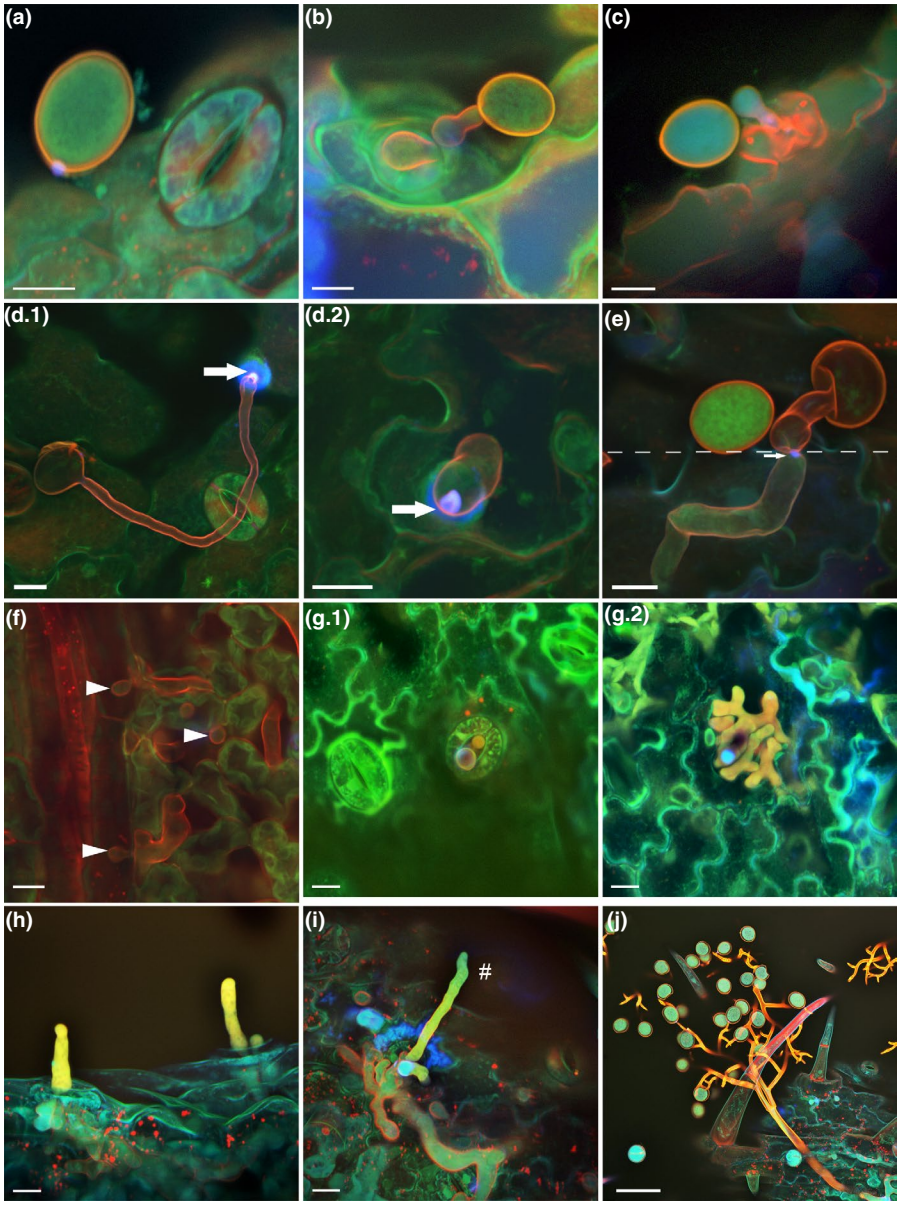


**FIGURE 2** Confocal laser scanning microscopy images of the asexual development of *Peronospora salviae-officinalis* on *Salvia officinalis* from 1 to 7 days after infection, stained with a 1:1 mixture of aniline blue and trypan blue. (a) Conidium on lower leaf surface of common sage next to a stoma. The callose plug sealing the base appears blue, indicating accumulation of β-(1,3)-glucans. (b) Conidium germinated with germ tube and appressorium. (c) Side view of an appressorium entering a stoma with an infection hypha. (d.1) Conidium germinated with a germ tube, directly penetrating the cuticule and epidermis. The plant accumulates callose around the penetration site, indicated by an arrow. (d.2) After entering the leaf tissue via the epidermis, *P. salviae-officinalis* develops a primary vesicle inside the plant tissue under the point of entry. (e) Side view of a germinated conidium, which enters the plant tissue directly via the epidermis. On the epidermis of the lower leaf surface (above the dotted line), the conidium forms a germ tube and penetrates the epidermis. Inside the leaf tissue (below the dotted line), directly under the epidermis, an intercellular hypha formed. (f) Haustoria, indicated by closed arrow heads, along leaf vein and in mesophyll cells, expanding in the plant cells from an intercellular hypha. (g.1) and (g.2) Images of a developing conidiophore primordium, at two focal planes. (g.1) On the leaf surface the conidiophore primordium is visible. (g.2) Inside the leaf tissue strong hyphal ramification under the stoma is visible. (h) and (i) Young conidiophores, indicated by a hash in (i) expanding from stomata. (j) Mature conidiophore between leaf hairs and glandular hairs with glandular cells of the leaf. Scale: (a–e) and (g–i) 10 μm; (f) 20 μm; (j) 50 μm. The physical depth of the *z* stack was as follows for each picture: (a) 4.5 μm; (b) 1 μm; (d.1) 1 μm; (d.2) 1.5 μm; (e) 21.84 μm; (f) 5.2 μm; (g.1) 3.12 μm; (g.2) 11.4 μm; (h) 46 μm; (i) 21 μm; and (j) 8 μm

TB 20, due to the quenching feature of trypan blue. The reduced autofluorescence led to a high resolution and strong visual contrast. The usage of two detectors to capture emission from the 561 nm laser increased the contrast between cytoplasm and cell wall of plant and oomycete. The overlay of green and red pseudocolours generated the pseudocolour yellow, resulting in a light to dark orange surface of intercellular hyphae. Thus, cell structures of the downy mildew were easily localized within the plant tissue. Early

development of a callose sheath around the haustorial neck could be distinguished from the entire encapsulation of older haustoria. The emission wavelength range was extended to enhance the brightness of hyphae in thicker samples without turning up laser intensity to avoid photobleaching.

### 3.2 | Histological study of *P. salviae-officinalis* infection of sage

After optimization, the CLSM visualization method was applied for a histological study of *P. salviae-officinalis* on *S. officinalis* in order to document the infection process from the adhesion of conidia on the leaf surface to de novo sporulation. The infection process began with an ovoid multinucleate conidiosporangiocyst, generally referred to as a conidium, attaching to the leaf surface of *S. officinalis*. The conidium displayed the typical callose plug sealing at the base where it had been attached to the conidiophore (Figure 2a). Conidia of *P. salviae-officinalis* germinate with a germ tube, which then develops an appressorium (Figure 2b) by inflating its tip, and from which a penetration hypha develops. Infection of the leaf tissue frequently occurs through a stoma (Figure 2c), but epidermal cells can also be penetrated directly (Figure 2d.1), probably by cell wall-degrading enzymes secreted at the hyphal apex (Hardham, 2007). In reaction to the penetration, the plant reinforces the cell wall by secreting callose at the point of entry (Figure 2d.1,d.2, arrow). In the intercellular space, *P. salviae-officinalis* forms a primary vesicle (Figure 2d.2), from which hyphae spread between the mesophyll cells (Figure 2e) and develop first haustoria (Figure 2f, closed arrow heads). Haustoria penetrate the host cell wall and invaginate the plasma membrane of the plant cell. In all observations, only a single haustorium was present per host cell. Occasionally an immune response of single plant cells was observed. Callose deposition and accumulation are found predominantly around haustoria, although most haustoria have little callose around them (Figure 3). Four days after inoculation intercellular hyphae were widespread between the mesophyll cells, and numerous intracellular globose haustoria inside the mesophyll cells could be observed (Figure 3) as well as the first persistent conidiosporangiophores, generally referred to as conidiophores.

Before forming a conidiophore, the intercellular hyphae branched strongly beneath a stoma, grew into the stomatal groove and formed a balloon-like structure, the conidiophore primordium (Figure 2g.1,g.2), which might have helped to keep the stoma open during initial conidiophore elongation. The conidiophore primordium developed into a conidiophore and emerged through the stoma. Usually one, but occasionally two to four, conidiophores emerged from a single stoma (Figure 2h,i). Mature conidiophores bore numerous conidia on multiple ramified branches (Figure 2j). Conidiophores of *P. salviae-officinalis* were not only, typically, observed on the lower side of the leaf but also on the upper side, because leaves of *S. officinalis* are amphistomatic. Seven days after inoculation many conidiophores with conidia were observed on the lower leaf surface and also some on the upper leaf surface. Conidia were then liberated and released actively into the air by twisting hygroscopic movements of

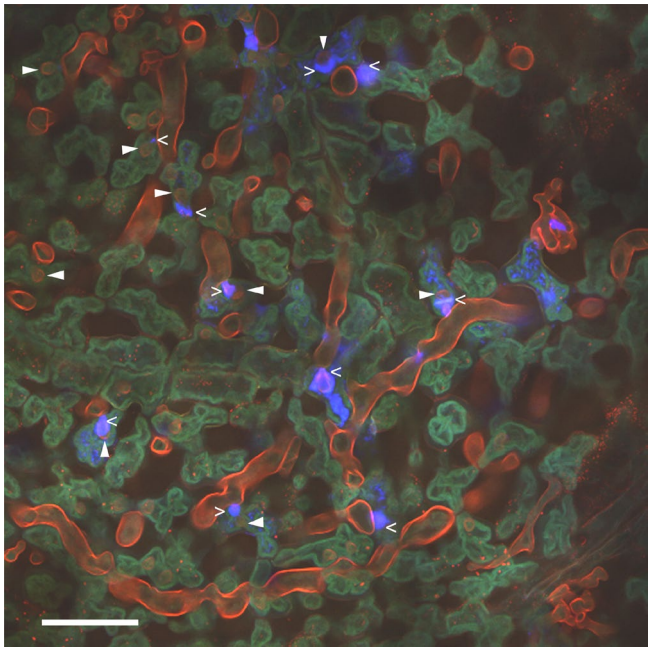

**FIGURE 3** Confocal laser scanning microscopy image of leaf tissue of *Salvia officinalis* infected by *Peronospora salviae-officinalis* 4 days after inoculation, stained with a 1:1 mixture of aniline blue and trypan blue. Intercellular hyphae are growing between leaf mesophyll cells. Strong ramification of the hyphae indicates points of conidiophore development. Numerous haustoria, indicated by closed arrow heads, are formed inside the mesophyll cells. Callose deposition around the necks of the haustoria (open arrow heads), a form of plant immune response, has already started. Scale: 20 µm. Physical depth of the *z* stack 1.5 µm

conidiophores upon drying (Lange *et al*., 1989). While sage leaf tissue was already colonized extensively by intercellular hyphae of *P. salviae-officinalis* 4 days after inoculation, chlorotic leaf spots were observed on infected sage leaves 7 days after inoculation at the earliest.

With the start of the homothallic sexual reproduction of *P. salviae-officinalis*, intercellular hyphae formed oogonia and antheridia. The antheridium formed a collar-like structure after penetration through the oogonium (Figure 4a). The antheridium stayed attached to the oogonium (Figure 4b,c) and formed a fertilization tube (Figure 4b, arrow) to transfer its haploid nuclei into the oosphere. Oospores were often formed directly under the cuticle, probably to promote their release after decomposition of the host tissue.

### 3.3 | Validation of the optimized staining method with samples of *P. lamii* on *L. purpureum* and *P. belbahrii* on *O. basilicum*

The optimized staining and CLSM visualization method was also tested on *P. lamii* parasitizing *L. purpureum* (red dead-nettle) and *P. belbahrii* parasitizing *O. basilicum* (basil) (Figure 5). All structures of *P. lamii* and *P. belbahrii* were visualized with similar quality as was shown for *P. salviae-officinalis* on *S. officinalis*. Consistent with the CLSM images taken from *P. salviae-officinalis*, cell walls

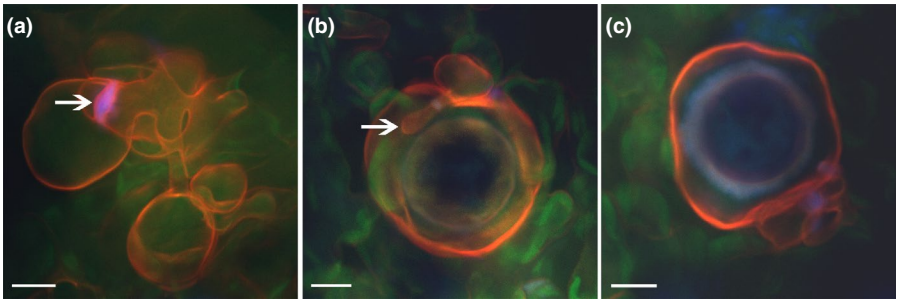


**FIGURE 4** Confocal laser scanning microscopy images of the sexual development of *Peronospora salviae-officinalis* on *Salvia officinalis*, 14 days after infection, stained with a 1:1 mixture of aniline blue and trypan blue. (a) Oogonium and antheridium formed by intercellular hyphae. The oogonium has been penetrated by an antheridium. The antheridium has formed a fertilization tube growing towards the oogonium (arrow). (b) Oospore with attached antheridium and fertilization tube. (c) Mature oospore with attached antheridium. Scale bars: 10 μm. The physical depth of the *z* stack was as follows for each picture: (a) 7.3 μm; (b) 16.6 μm; (c) 5.2 μm

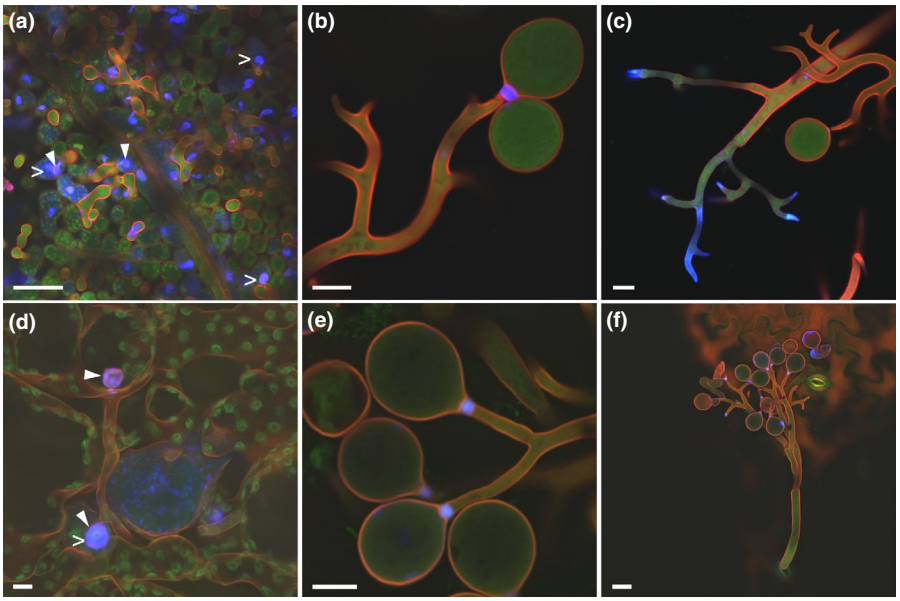


**FIGURE 5** Confocal laser scanning microscopy images of *Peronospora lamii* on *Lamium purpureum* and of *Peronospora belbahrii* on *Ocimum basilicum* stained with a 1:1 mixture of aniline blue and trypan blue. (a–c) *P. lamii on L. purpureum*. (a) Intercellular hyphae and haustoria. Callose is deposited around the necks of haustoria and some haustoria are already encapsulated by callose. (b) Ultimate branchlets of a conidiophore with two conidia. A callose plug is formed between one conidium and the end of the branch, at the abscission site of the conidium. The blue colour indicates that the plug contains β-(1,3)-glucans. (c) Branches of a conidiophore, showing older parts of the conidiophore with dense deposition of β-(1,3)-glucans at abscission sites. Younger parts are without deposition of β-(1,3)-glucan. (d–f) *P. belbahrii* on *O. basilicum*. (d) Intercellular hyphae between mesophyll cells with two intracellular haustoria. Callose deposition has begun and one haustorium is encapsulated in callose. (e) Conidia of *P. belbahrii* on the ultimate branchlets of a conidiophore. Plugs with β-(1,3)-glucans are formed at the abscission site. (f) Conidiophore of *P. belbahrii* emerging from a stoma. (a, d) Haustoria are indicated by a closed arrow head, callose deposition by an open arrow head. Scale: (a) 50 μm, (b–d) 10 μm. The physical depth of the *z* stack was as follows for each picture: (c) 6 μm; (d) 10 μm; (f) 10 μm

of intercellular hyphae, conidia, and conidiophores appeared red-orange, cytoplasm was yellow to green, and callose appeared blue (Figure 5a,d). Within infected leaf tissue of basil and red dead-nettle, callose accumulation around haustoria was also observed. Like *P. salviae-officinalis*, conidia of *P. lamii* and *P. belbahrii* have a callose plug at their base where they are attached to the end branches of the conidiophore, but the plugs of *P. lamii* and *P. belbahrii* are very thick (Figure 5b,c,e,f). The strong blue signal indicates that the plug contains large amounts of β-(1,3)-glucans. Branches of conidiophores of *P. lamii* from which the sporangia were already discharged also showed strong blue signals (Figure 5c). The signal is probably a reflection of either sealing of the conidiophore upon plasma retreat or a side-effect of drying.

## 4 | DISCUSSION

Fluorescence staining and imaging of oomycete–plant interactions is challenging due to the similarity in cell wall composition of both plant and microorganism, with β-1,3 bond glucose units as the dominating cell

wall components. Because large amounts of chitin are absent from most oomycete cell walls, staining protocols used for true fungi cannot be applied. The staining procedure for CLSM of *Peronospora* species infective to Lamiaceae presented here, involving decolourization with ethanol and KOH and staining with a 1:1 aniline blue–trypan blue mixture, allows detailed visualization of downy mildew structures outside and inside the host tissue, as well as of callose deposition as an immune response of the plant.

One of the major advantages of confocal microscopy is the non-invasive quality of optical sectioning (Czymmek *et al*., 1994). With our protocol, embedding or fixation of samples is not necessary, preserving a natural tissue structure. While pure trypan blue staining has frequently been used and resulted in sufficient resolution for the visualization of oomyceteous hyphae in the thin cotyledons and leaves of *Arabidopsis thaliana* (Huitema *et al*., 2003; Robinson and Cahill, 2003; Takemoto *et al*., 2003), it resulted in blurred pictures of the oomycetous structures within sage leaves. The method developed here overcame this problem and can also be used in thicker and more complex tissues. Callose deposition within infected leaf tissue was not observed in studies where only trypan blue was used for staining (Huitema *et al*., 2003; Takemoto *et al*., 2003). However, it has been shown that callose encasements around haustoria can be detected when stained with aniline blue (Rumbolz *et al*., 2002; Dong *et al*., 2008). This is the first study where aniline blue and trypan blue have been used simultaneously. This increases the resolution of oomycete and plant structures significantly compared to studies where either have been employed alone (Donofrio and Delaney, 2001; Robinson and Cahill, 2003). The dual staining with aniline blue and trypan blue enabled the clear visualization of oomycete and plant structures, such as the downy mildew infection structures and callose deposition as a result of host defence responses to pathogen infection. With aniline blue alone, infection structures as well as callose deposition were also visible, but it was more difficult to distinguish between plant and oomycete structures. In contrast, callose cannot be visualized with trypan blue, but it is easier to distinguish structures of *Peronospora* from plant cells than with aniline blue staining. Although oomycete structures inside the plant tissue could be observed in decolourized but unstained samples, ample experience of microscopic observation of intercellular hyphae or haustoria is necessary for their distinction.

In addition to the combination of aniline blue and trypan blue in this study, three detectors were used to capture the emission fluorescence of plant and oomycete tissue: the photomultiplier tubes PMT2 (447–495 nm) and PMT4 (673–749 nm) and the hybrid detector HyD3 (593–625 nm). The signals were displayed in different pseudocolours: PMT2 in blue, HyD3 in green, and PMT4 in red pseudocolour. The merged images show an overlay of all three channels. The overlay of green and red pseudocolours generates the pseudocolour yellow, resulting in a light to dark orange surface of intercellular hyphae. The intensity and shade of the signal can vary, depending on the angle the image is taken and the number of overlying stacks. These additional pseudocolour shades improve visualization so that cell structures of downy mildew pathogens embedded within the plant tissue can be readily visualized for their localization. For example, developing, thin encapsulations of haustoria can be distinguished from the entire encapsulation of older haustoria, because the red structure of the haustorium itself is visible through the blue callose layer, whereas the haustoria cannot be seen through the thick callose layer after complete encapsulation.

Using the optimized method developed here, we tracked the infection of *S. officinalis* by *P. salviae-officinalis* from adhesion of conidia on the leaf surface to sporulation. This is the first study illustrating the whole asexual, as well as sexual, cycle of the development of *P. salviae-officinalis*. Moreover, it was also possible to detect callose deposition and accumulation by the plant in downy mildew-infected leaf tissue of sage, basil, and red dead-nettle. Callose depositions are a well-known, nonspecific immune response of plants towards mechanical and pathogenic injury (Kortekamp, 2005; Judelson and Ah-Fong, 2019). Encapsulations of haustoria by callose are known for several downy mildew infections, such as *Plasmopara viticola* on *Vitis vinifera*, *Bremia lactucae* on *Lactuca sativa* (Sedlarova and Lebeda, 2001; Kortekamp, 2005; Diez-Navajas *et al*., 2008), and *Peronospora parasitica* and *Hyaloperonospora arabidopsidis* on *A. thaliana* (Donofrio and Delaney, 2001; Fabro *et al*., 2011). Assessment of callose depositions around haustoria have been used to evaluate the performance of an effector, or to determine host defence responses as a degree of resistance in a crop cultivar towards downy mildew infections. For this, aniline blue staining of callose depositions is often used (Donofrio and Delaney, 2001; Diez-Navajas *et al*., 2008; Fabro *et al*., 2011; Caillaud *et al*., 2012). Haustorial encasements are double-layered, with callose-containing membrane structures that often surround older haustoria as part of cellular host defence. In compatible interactions the encapsulation of haustoria is delayed and lags behind the spread of the pathogen (Lu *et al*., 2012). It is assumed that encasements restrict the nutrient uptake by the pathogen, impair effector translocation, or concentrate plant-derived antimicrobials. Oomycetes, on the other hand, have developed countermeasures against this plant defence system to secure their nutrient source (Judelson and Ah-Fong, 2019). We found that in the case of *P. salviae-officinalis*, just a few of the numerous haustoria formed possessed a callose collar around the neck or were encapsulated by callose. For *H. arabidopsidis*, it has been reported that this pathogen employs several effectors to suppress the deposition of callose by *A. thaliana* (Fabro *et al*., 2011). In addition, other downy mildews, such as *Plasmopara halstedii* parasitizing sunflowers, are known to mask their pathogen-associated molecular patterns, or are capable of down-regulating the immune response (Sharma *et al*., 2015). Further investigation is needed to determine whether the rather low amount of callose around haustoria in our study was due to the juvenility of these haustoria or if this was a result of a suppressed immune response. Nevertheless, the low abundance of callose depositions and the late formation of chlorotic or necrotic leaf spots in infected plants indicate that *P. salviae-officinalis* is well adapted to its host.

## ACKNOWLEDGEMENTS

This study was funded with support from the Federal Ministry of Food and Agriculture by decision of the German Bundestag.

## DATA AVAILABILITY STATEMENT

The data sets generated and analysed during the current study are available from the corresponding author on reasonable request.

## ORCID

*Mascha Hoffmeister* https://orcid.org/0000-0001-5500-9270
*Wolfgang Maier* https://orcid.org/0000-0002-2531-6998
*Marco Thines* https://orcid.org/0000-0001-7740-6875
*Yvonne Becker* https://orcid.org/0000-0002-5920-8581

## REFERENCES

Avelar-Freitas, B.A., Almeida, V.G., Pinto, M.C., Mourão, F.G., Massensini, A.R., Martins-Filho, O.A. *et al*. (2014) Trypan blue exclusion assay by flow cytometry. *Brazilian Journal of Medical and Biological Research*, 47, 307–315.

Bartnicki-Garcia, S. (1968) Cell wall chemistry, morphogenesis, and taxonomy of fungi. *Annual Review of Microbiology*, 22, 87–108.

Beakes, G. and Thines, M. (2017) Hyphochytriomycota and oomycota. In: Archibald, J.M., Simpson, A.G.B. and Slamovits, C.H. (Eds.) *Handbook of the Protists*. Cham, Switzerland: Springer, pp. 435–506.

Becker, Y., Green, K., Scott, B. and Becker, M. (2018) Artificial inoculation of *Epichloe festucae* into *Lolium perenne*, and visualisation of endophytic and epiphyllous fungal growth. *Bioprotocols*, 8, e2990.

Belbahri, L., Calmin, G., Pawlowski, J. and Lefort, F. (2005) Phylogenetic analysis and real time PCR detection of a presumably undescribed *Peronospora* species on sweet basil and sage. *Mycological Research*, 109, 1276–1287.

Blaschek, W.K.J., Kraus, J. and Franz, G. (1992) *Pythium aphanidermatum*: culture, cell-wall composition, and isolation and structure of antitumour storage and solubilised cell-wall (1→3), (1→6)-β-D-glucans. *Carbohydrate Research*, 231, 293–307.

Bougourd, S., Marrison, J. and Haseloff, J. (2000) Technical advance: an aniline blue staining procedure for confocal microscopy and 3D imaging of normal and perturbed cellular phenotypes in mature *Arabidopsis* embryos. *The Plant Journal*, 24, 543–550.

Caillaud, M.C., Piquerez, S.J. and Jones, J.D. (2012) Characterization of the membrane-associated HaRxL17 Hpa effector candidate. *Plant Signaling & Behavior*, 7, 145–149.

Choi, Y.J., Shin, H.D. and Thines, M. (2009) Two novel *Peronospora* species are associated with recent reports of downy mildew on sages. *Mycological Research*, 113, 1340–1350.

Clavaud, C., Aimanianda, V. and Latge, J.P. (2009). Organization of fungal, oomycete and lichen (1,3)-β-glucans. In: Bacic, A.F., Fincher, G.B. and Stone, B.A. (Eds.) *Chemistry, Biochemistry and Biology of (1–3)-β-glucans and Related Polysaccharides*. Amsterdam, Netherlands: Elsevier, pp. 387–424.

Combes, R.D. and Haveland-Smith, R.B. (1982) A review of the genotoxicity of food, drug and cosmetic colours and other azo, triphenylmethane and xanthene dyes. *Mutation Research*, 98, 101–248.

Czymmek, K.J., Whallon, J.H. and Klomparens, K.L. (1994) Confocal microscopy in mycological research. *Experimental Mycology*, 18, 275–293.

Diez-Navajas, A.M., Greif, C., Poutaraud, A. and Merdinoglu, D. (2007) Two simplified fluorescent staining techniques to observe infection structures of the oomycete *Plasmopara viticola* in grapevine leaf tissues. *Micron*, 38, 680–683.

Diez-Navajas, A.M., Wiedemann-Merdinoglu, S., Greif, C. and Merdinoglu, D. (2008) Nonhost versus host resistance to the grapevine downy mildew, *Plasmopara viticola*, studied at the tissue level. *Phytopathology*, 98, 776–780.

Dong, X., Hong, Z., Chatterjee, J., Kim, S. and Verma, D.P. (2008) Expression of callose synthase genes and its connection with Npr1 signaling pathway during pathogen infection. *Planta*, 229, 87–98.

Donofrio, N.M. and Delaney, T.P. (2001) Abnormal callose response phenotype and hypersusceptibility to *Peronospora parasitica* in defence-compromised *Arabidopsis nim1-1* and salicylate hydroxylase-expressing plants. *Molecular Plant-Microbe Interactions*, 14, 439–450.

Eschrich, W. and Currier, H.B. (2009) Identification of callose by its diachrome and fluorochrome reactions. *Stain Technology*, 39, 303–307.

Fabre, I.B., Bruneteau, M., Ricci, P. and Michel, G. (1984) Isolement et étude structurale de glucanes de *Phytophthora parasitica*. *European Journal of Biochemistry*, 142, 99–103.

Fabro, G., Steinbrenner, J., Coates, M., Ishaque, N., Baxter, L., Studholme, D.J. *et al*. (2011) Multiple candidate effectors from the oomycete pathogen *Hyaloperonospora arabidopsidis* suppress host plant immunity. *PLoS Pathogens*, 7, e1002348.

Gamliel, A. and Yarden, O. (1998) Diversification of diseases affecting herb crops in Israel accompanies the increase in herb crop production. *Phytoparasitica*, 26, 53–58.

Gindro, K., Pezet, R. and Viret, O. (2003) Histological study of the responses of two *Vitis vinifera* cultivars (resistant and susceptible) to *Plasmopara viticola* infections. *Plant Physiology and Biochemistry*, 41, 846–853.

Hardham, A.R. (2007) Cell biology of plant–oomycete interactions. *Cellular Microbiology*, 9, 31–39.

Hill, C.F., Pearson, H.G. and Gill, G.S.C. (2004) *Peronospora dianthi* and *Peronospora lamii*, two downy mildews recently detected in New Zealand. *New Zealand Plant Protection*, 57, 348.

Hood, M.E. and Shew, H.D. (1996) Applications of KOH aniline blue fluorescence in the study of plant–fungal interactions. *Phytopathology*, 86, 704–708.

Huitema, E., Vleeshouwers, V.G., Francis, D.M. and Kamoun, S. (2003) Active defence responses associated with non-host resistance of *Arabidopsis thaliana* to the oomycete pathogen *Phytophthora infestans*. *Molecular Plant Pathology*, 4, 487–500.

Humphreys-Jones, D.R., Barnes, A.V. and Lane, C.R. (2008) First report of the downy mildew *Peronospora lamii* on *Salvia officinalis* and *Rosmarinus officinalis* in the UK. *Plant Pathology*, 57, 372.

Judelson, H.S. and Ah-Fong, A.M.V. (2019) Exchanges at the plant–oomycete interface that influence disease. *Plant Physiology*, 179, 1198–1211.

Kortekamp, A. (2005) Growth, occurrence and development of septa in *Plasmopara viticola* and other members of the Peronosporaceae using light- and epifluorescence-microscopy. *Mycological Research*, 109, 640–648.

Lange, L., Eden, U. and Olson, L.W. (1989) Zoosporogenesis in *Pseudoperonospora cubensis*, the causal agent of cucurbit downy mildew. *Nordic Journal of Botany*, 8, 497–504.

Liberato, J.R., Forsberg, L., Grice, K.R. and Shivas, R.G. (2006) *Peronospora lamii* on Lamiaceae in Australia. *Australasian Plant Pathology*, 35, 367–368.

Liesche, J., Marek, M. and Gunther-Pomorski, T. (2015) Cell wall staining with trypan blue enables quantitative analysis of morphological changes in yeast cells. *Frontiers in Microbiology*, 6, 107.

Lu, Y.-J., Schornack, S., Spallek, T., Geldner, N., Chory, J., Schellmann, S. *et al*. (2012) Patterns of plant subcellular responses to successful oomycete infections reveal differences in host cell reprogramming and endocytic trafficking. *Cellular Microbiology*, 14, 682–697.

McMillan, R.T. (1993) First report of downy mildew of *Salvia* in Florida. *Plant Disease*, 78, 317.

Mosiman, V.L., Patterson, B.K., Canterero, L. and Goolsby, C.L. (1997) Reducing cellular autofluorescence in flow cytometry: an *in situ* method. *Cytometry*, 30, 151–156.

Mulisch, M. and Welsch, U. (2015) *Romeis – Mikroskopische Technik*. Berlin, Germany: Springer.

Robinson, L.H. and Cahill, D.M. (2003) Ecotypic variation in the response of *Arabidopsis thaliana* to *Phytophthora cinnamomi*. *Australasian Plant Pathology*, 32, 53–64.

Rumbolz, J., Wirtz, S., Kassemeyer, H.H., Guggenheim, R., Schafer, E. and Buche, C. (2002) Sporulation of *Plasmopara viticola*: differentiation and light regulation. *Plant Biology*, 4, 413–422.

Sedlarova, M. and Lebeda, A. (2001) Histochemical detection and role of phenolic compounds in the defense response of *Lactuca* spp. to lettuce downy mildew (*Bremia lactucae*). *Journal of Phytopathology*, 149, 693–697.

Sharma, R., Xia, X., Cano, L.M., Evangelisti, E., Kemen, E., Judelson, H. *et al*. (2015) Genome analyses of the sunflower pathogen *Plasmopara halstedii* provide insights into effector evolution in downy mildews and *Phytophthora*. *BMC Genomics*, 16, 741.

Sietsma, J.H., Eveleigh, D.E. and Haskins, R.H. (1969) Cell wall composition and protoplast formation of some oomycete species. *Biochimica et Biophysica Acta*, 184, 306–317.

Smith, M.M. and McCully, M.E. (1978) A critical evaluation of the specificity of aniline blue induced fluorescence. *Protoplasma*, 95, 229–254.

Stone, B.A., Evans, N.A., Bonig, I. and Clarke, A.E. (1984) the application of sirofluor, a chemically defined fluorochrome from aniline blue for the histochemical detection of callose. *Protoplasma*, 122, 191–195.

Takemoto, D., Jones, D.A. and Hardham, A.R. (2003) GFP-tagging of cell components reveals the dynamics of subcellular re-organization in response to infection of *Arabidopsis* by oomycete pathogens. *The Plant Journal*, 33, 775–792.

Thines, M. and Choi, Y.J. (2016) Evolution, diversity, and taxonomy of the Peronosporaceae, with focus on the genus *Peronospora*. *Phytopathology*, 106, 6–18.

Thines, M., Goker, M., Oberwinkler, F. and Spring, O. (2007) A revision of *Plasmopara penniseti*, with implications for the host range of the downy mildews with pyriform haustoria. *Mycological Research*, 111, 1377–1385.

Wood, P.J. and Fulcher, R.G. (1984) Specific interaction of aniline blue with (1→3)-β-D-glucan. *Carbohydrate Polymers*, 4, 49–72.

Yamada, M. and Miyazaki, T. (1976) Ultrastructure and chemical analysis of the cell wall of *Pythium debaryanum*. *Japanese Journal of Microbiology*, 20, 83–91.

## SUPPORTING INFORMATION

Additional supporting information may be found online in the Supporting Information section.

**How to cite this article:** Hoffmeister M, Maier W, Thines M, Becker Y. Tracking host infection and reproduction of *Peronospora salviae-officinalis* using an improved method for confocal laser scanning microscopy. *Plant Pathol*. 2020;69:922–931. https://doi.org/10.1111/ppa.13173